Significant Reduction of the Loop Current in the 21st Century and Its Impact on the Gulf of Mexico

Yanyun Liu[1,2], Sang-Ki Lee[1,2], Barbara A. Muhling[1,3], John T. Lamkin[3], and David B. Enfield[1,2]

[1]Cooperative Institute for Marine and Atmospheric Studies, University of Miami, Miami, Florida, USA

[2]Atlantic Oceanographic and Meteorological Laboratory, NOAA, Miami, Florida, USA

[3]Southeast Fisheries Science Center, NOAA, Miami, Florida, USA

2nd Revision to Journal of Geophysical Research-Oceans

April 2012

Corresponding author address: Yanyun Liu, NOAA/AOML, 4301 Rickenbacker Causeway, Miami, FL 33149, USA. E-mail: Yanyun.Liu@noaa.gov.

Abstract

This study examines the potential impact of future anthropogenic global warming on the Gulf of Mexico (GoM) by using a downscaled high-resolution ocean model constrained with the surface forcing fields and initial and boundary conditions obtained from the IPCC-AR4 model simulations under A1B scenario. The simulated volume transport by the Loop Current (LC) is reduced considerably by 20 - 25% during the 21st century, consistent with a similar rate of reduction in the Atlantic Meridional Overturning Circulation. The effect of the LC in the present climate is to warm the GoM, therefore the reduced LC and the associated weakening of the warm LC eddy have a cooling impact in the GoM, particularly in the northern basin. Due to this cooling influence, the northern GoM is characterized as the region of minimal warming. Low-resolution models, such as the IPCC-AR4 models, underestimate the reduction of the LC and its cooling effect, thus fail to simulate the reduced warming feature in the northern GoM. The potential implications of the reduced warming in the northern GoM on pelagic fish species and their spawning patterns are also discussed.

1. Introduction

The IPCC-AR4 climate model simulations under A1B scenario project that the upper ocean temperature in the North Atlantic Ocean may increase by approximately 2^{o}C and the Atlantic Meridional Overturning Circulation (AMOC) may slow down by about 25% during the 21st century [e.g., Schmittner et al., 2005; Drijfhout and Hazeleger, 2006]. Both the increased North Atlantic upper ocean temperature and the decreased AMOC may have strong impacts on the Atlantic marine ecosystem, resulting in substantial reduction of productivity in the Atlantic Ocean owing to reduced upwelling of nutrient-rich deep water and the gradual depletion of upper-ocean nutrient concentration [e.g., Schmittner, 2005].

Atlantic bluefin tuna (BFT) is one such species that can be greatly affected by future climate change in the Gulf of Mexico (GoM). The spawning of BFT has been recorded predominantly in the northern GoM from April to June (AMJ) with the optimal spawning temperature of 24 - 27^{o}C [e.g., Schaefer 2001]. Adult BFTs are adversely affected by warm water (>28°C) and thus avoid warm features in the GoM such as the Loop Current [Blank et al. 2004]. A recent study analyzed the IPCC-AR4 climate model simulations to show that areas in the northern GoM with high probabilities of larval occurrence could be substantially reduced by the end of the 21st century because the increased upper ocean temperature would no longer support the optimal spawning conditions [Muhling et al., 2011]. BFTs are therefore likely to be vulnerable to climate change, suggesting that there is potential for significant changes in their spawning and migration behaviors.

Because the Loop Current (LC) in the GoM is a part of the North Atlantic western boundary currents system and is an important pathway of the AMOC, it is expected that the LC be reduced as the AMOC slows down in the 21st century. Since the advective ocean heat convergence associated with the LC is an important mechanism to offset the surface cooling in the GoM, the reduced LC should play an important role in the projected surface warming in the GoM. However, the IPCC-AR4 climate models have typical spatial resolution of about 1^o. As demonstrated by Oey et al. [2005], 1^o resolution is too coarse to properly resolve the strength, position and eddy shedding characteristics of the LC. Thus, here we use a downscaled high-resolution ocean model to assess the potential impact of future anthropogenic global warming (AGW) on the GoM, with a particular focus on AMJ, the spawning season for BFT.

2. Model and Model experiments

The Miami Isopycnic Coordinate Ocean Model (MICOM) version 2.8 is used as the downscaling model in this study. As described in Bleck et al. [1992], the surface mixed layer is modeled by a bulk mixed layer in MICOM, while the turbulent mixing across the mixed layer base is explicitly computed using the turbulence energy equation of Gaspar [1988].

Ocean-only models, such as MICOM, are usually forced with prescribed atmospheric conditions. Typically, flux forms of atmospheric forcing, such as short and long wave radiative heat fluxes, precipitation rate and wind stress, are directly used to force an ocean-only model. For latent and sensible heat fluxes, however, bulk equations are typically used to compute them interactively using wind speed, air humidity and air temperature at 10m (or 2m) along with the model SST. Such a treatment of the turbulent heat fluxes ultimately relaxes the model SST toward the prescribed surface air temperature. However, since our main objective in this study is to explore how the IPCC-AR4 projected SST changes are modified by resolving important regional ocean dynamic features in the GoM, it is not proper to use the conventional surface forcing scheme to damp the ocean model SST toward that of the IPCC-AR4 model simulations.

An effective way to allow an ocean-only model to have physically consistent heat and freshwater exchanges at the air-sea interface is to couple it with an atmospheric mixed layer model (AML) of Seager et al. [1995] which solves the advection-diffusion equations for air temperature and humidity in the planetary boundary layer (PBL). Therefore, in this study, the MICOM is coupled to the AML (MICOM-AML). Coupling the MICOM with the AML allows physically consistent heat and freshwater exchanges at the air-sea interface, and thus prevents the model SSTs from simply damping toward the IPCC-AR4 model SSTs. The air temperature and humidity above the PBL and the wind vector fields in the PBL, which are needed for the coupled MICOM, are obtained from the IPCC-AR4 model simulations under 20C3M (from 1900 to 2000) and A1B (from 2000 to 2100) scenarios.

Two additional and necessary changes are added to the MICOM. First, the detrainment algorithm is revised following Lee et al. [2007] to suppress spurious warming of the mixed layer induced by detrainment. Second, the shear-driven vertical mixing scheme of Price-Weller-Pinkel (PWP) [Price et al. 1986] is added in such a way that the heat, salt and momentum in the subsurface layer are entrained into the surface mixed layer until the critical bulk Richardson number reaches 1.0 [Jaimes et al., 2011].

Sixteen isopycnic layers are used with density values of 31.82, 33.19, 34.23, 35.01, 35.59, 35.98, 36.27, 36.49, 36.66, 36.79, 36.89, 36.98, 37.04, 37.08, 37.11 and 37.14. The first layer is the surface mixed layer, thus the density changes in time and space. The main reason for using the density coordinate is to preserve the thermodynamic properties of water mass, and thus to minimize the numerically induced diapycnal mixing. The MICOM-AML model is driven by surface forcing fields obtained from the IPCC-AR4 model simulations, including surface wind stress, air temperature, specific humidity, shortwave and longwave radiation, and precipitation fields. The sea surface salinity (SSS) of the model is relaxed toward the SSS of the IPCC-AR4 model simulations to account for the processes not explicitly considered in our model simulations, such as the river run-off. Note that in ocean-only models, SSS relaxation is a common practice to account for freshwater fluxes not explicated simulated, such as those associated with seaice formation/melting and river run-off [e.g., Chassignet et al. 1996]. In particular, as discussed in Griffies et al. [2009], ocean general circulation models do require a salinity restoring to simulate the observed strength of the AMOC. The initial and boundary conditions are obtained from the weighted ensembles of the IPCC-AR4 model simulations under the two scenarios as described in the next section.

We performed two sets of model experiments, one with a low-resolution MICOM-AML and the other using a version with high resolution. For both experiments, the model domain contains the Atlantic Ocean between 100^o W and 20^o E bounded north and south by 65^o N and 20^o S, respectively. The low-resolution model experiment (EXP_LR) has a horizontal resolution of 1^o, which is the typical horizontal resolution of the IPCC-AR4 ocean models, and thus cannot fully resolve the strength, position and eddy shedding characteristics of the LC. The high-resolution model (EXP_HR) has the fully eddy-resolving horizontal resolution of 0.1^o over the GoM region from 10^oN to 30^oN and from 100^oW to 70^oW decreasing linearly to 0.25^o in the rest of the model domain.

For both the low- and high-resolution configurations, three sets of experiments are conducted for three different periods, namely the late-20th century (from 1981 to 2000), the mid-21st century (from 2041 to 2060) and the late-21st century (from 2081 to 2100). All three sets of experiments are initialized and integrated for 20 years by constraining the MICOM-AML with the surface forcing fields and initial and boundary conditions derived from the IPCC-AR4 model simulations for the corresponding time periods. For each model simulation, the first 10 years of model outputs are discarded to exclude any potentially spurious spin-up effect.

In order to minimize the biases in the surface forcing fields obtained from the IPCC-AR4 model simulations, we first construct the IPCC-AR4 climatology for the 1971-2000 periods, and then compute the difference between the IPCC-AR4 climatology and the observed surface forcing climatology. The Coordinated Ocean Research Experiments version-2 (CORE2) surface forcing product [Large and Yeager. 2008] is used to derive the observed surface forcing climatology. Then, the difference (i.e., the bias-correction term) is added to the IPCC-AR4 surface forcing fields for the three different periods. The initial and boundary conditions for the temperature and salinity are also bias-corrected following the same methodology used for the surface forcing fields. The observed temperature and salinity climatology are obtained from the U.S. Navy Generalized Digital Environmental Model version 3.0 (GDEM3) [Carnes, 2009]. Then, the difference between the IPCC-AR4 climatology and the observed (GDEM3) temperature and salinity climatology during the period of 1971-2000 is added to the IPCC-AR4 temperature and salinity for the three different periods.

3. Weighting the IPCC-AR4 models

Eleven IPCC-AR4 models are used to derive the surface forcing fields and initial and boundary conditions (see Table 1). These eleven IPCC-AR4 models are selected because they all show a realistic AMOC strength in the 20th century and contain all surface flux variables needed for the model experiments. Each of the eleven IPCC-AR4 models is ranked and weighted based on its ability to replicate the observed upper ocean temperature at the surface, 100m and 200m in the GoM for the last 30 years of the 20th century (1971-2000) for AMJ, the major spawning season for BFT. The observed upper ocean temperatures of the 20th century are derived from the GDEM3. Additionally, since the North Atlantic SSTs depend strongly on the AMOC for its effect on the northward advection of warm surface water [e.g., Schmittner, 2005], the AMOC strength based on the maximum overturning streamfunction at 30^{o}N is also used to rank and weight the IPCC-AR4 models. The AMOC strength at 30^{o} N is computed for each IPCC-AR4 model during 1971-2000 and compared to the observed value of $18.0 \pm 2.5\,\mathrm{Sv}$ [Lumpkin and Speer, 2007]. The same weight is given for all four indexes (three temperature levels and AMOC).

The weight coefficient is applied to the bias-corrected surface forcing fields and initial and boundary conditions of each IPCC-AR4 model (see Table 1). Then, their weighted ensemble averages are derived and used to perform the MICOM-AML experiments. See Muhling et al. [2011] for detailed description about the weighting of the IPCC-AR4 models. In all model experiments, the ocean boundaries at 65^{o}N and 20^{o}S are treated as closed, but are outfitted with about 5^{o} of buffer zones in which the temperature and salinity are linearly relaxed toward the corresponding IPCC-AR4 fields. Two additional buffer zones are located in the northwestern corner over the Labrador Sea, and in the Gulf of Cadiz (representing the Mediterranean Sea) as in Chassignet et al. [1996]. The restoring time scale for the northern and southern boundaries varies linearly from 25 days at the inner edge to 5 days at the walls. The timescale for the Labrador Sea region is 25 days and, for the Mediterranean Sea, 365 days.

4. Results

Figure 1 shows the SST difference in the GoM between the late 21st century and late 20th century in AMJ obtained from the weighted ensemble of IPCC-AR4 models and the MICOM experiments (EXP_LR and EXP_HR). The IPCC-AR4 models show that the GoM is warmed by more than 2^oC almost everywhere. The warming is particularly large in the northern GoM, which is the known spawning ground for BFT. This feature in the IPCC-AR4 models is reasonably well reproduced in EXP_LR. Further analysis shows that a subtle imbalance between the downward long-wave radiative flux and the latent heat flux is responsible for the large warming in the northern GoM in both the IPCC-AR4 model composite and EXP_LR (not shown). Here, we mainly focus on the late-20th century and the late-21st century experiments. The results from the mid-21st century experiment are largely consistent with the results from the late-21st century experiment, but with reduced amplitude in the change from the late-20th century experiment.

It is clear that the GoM is also warmed everywhere in EXP_HR, but the spatial pattern of the warming is quite different from the IPCC-AR4 model composite and EXP_LR. In particular, the SST increase in EXP_HR is much less in the northern GoM and a large warming is now confined to the region south of the Florida panhandle. In fact, the northern GoM away from the Florida west coast is now characterized as the region of minimum warming in EXP_HR, whereas it is a region of intense warming in both the IPCC-AR4 model composite and EXP_LR. The projected SST increase over this minimum warming region is only about $1 \sim 1.5^oC$ in EXP_HR, but it is more than 2^oC in EXP_LR. A potential cause for this difference may be the weakening of the LC and the associated reduction in the warm water transport through the Yucatan Channel, which are not well simulated in low-resolution models such as the IPCC-AR4 models and EXP_LR [e.g., Lee et al., 2005; Lee et al., 2007].

Figure 2a shows the long-term mean surface current obtained from EXP_HR during AMJ in the late 20th century with a large anticyclone feature in the northern GoM connected to the main branch of the LC. It is important to note that this feature is visible only in a long-term mean climatology and thus predominated by transient synoptic eddies in any given time (not shown). Figure 2b shows the surface current change in the GoM during AMJ between the late 21st century and the late 20th century obtained from EXP_HR. It is clear that the LC is much weakened (note that arrows are reversed from Figure 2a). It is noticed that an anomalous cyclonic ring (centered around 90^{o}W, 26^{o}N) is formed in the central and northern GoM. This feature indicates that the warm LC eddy detached from the main branch of the LC is weakened, and thus shallower (not shown) and colder.

To gain a better perspective of how the reduced LC is linked to the reduced warming feature in the northern GoM in EXP_HR, the surface mixed layer heat budget is diagnosed. The heat budget equation that governs the diabatic-heating rate in the bulk mixed layer can be written as

$$\underbrace{\rho c_p h_M \frac{\partial T_M}{\partial t}}_{Q_{STR(M)}} = \underbrace{R\big|_0 + Q_{LAT} + Q_{SEN}}_{Q_{NET}} \underbrace{- \rho c_p \mathbf{v}_M \cdot \nabla T_M}_{Q_{ADV(M)}} \underbrace{- w_e (T_M - T_e)}_{Q_{DIF(M)}}, \qquad (1)$$

where ρ is the seawater density (1027 kg/m^3), c_p is the specific heat of seawater (3990 J kg^{-1}K^{-1}), h_M, T_M, and $\mathbf{v}_M$ are the depth, temperature and velocity vector of the bulk mixed layer, respectively, w_e is the entrainment rate and T_e is the temperature of an isopycnal layer being entrained. The LHS is the heat storage rate ($Q_{STR(M)}$). The RHS includes the surface net heat flux (Q_{NET}), the advective heat flux convergence ($Q_{ADV(M)}$) and the turbulent heat flux (or entrainment cooling) across the mixed layer base ($Q_{DIF(M)}$), respectively. The surface net heat flux (Q_{NET}) includes the surface radiative heat flux ($R|_0$), the latent heat flux (Q_{LAT}) and the sensible heat flux (Q_{SEN}). The advective heat flux convergence term ($Q_{ADV(M)}$) contains only the horizontal component because vertical component does not explicitly contribute to diabatic heating. The horizontal sub-grid diffusion term is ignored because it is small. See Lee et al. [2007] for further discussion on how each term in (1) is related to corresponding term in a slab mixed layer heat budget equation.

Figure 3a and b show the anomalous surface heat flux and advective heat flux convergence in the GoM between the late 21st century and the late 20th century in March, April and May (MAM) obtained from EXP_HR. The turbulent mixing term is not shown because it is much smaller than these two terms. Here, we focus on MAM to understand the heat flux terms that lead to the reduced warming of the surface mixed layer in the northern GoM during AMJ. Note that the anomalous surface heat flux and advective heat flux convergence in February, March and April (FMA) are very similar to those shown in Figure 3a and b (not shown). It is clear that the reduced warming in the northern GoM is largely caused by anomalous advective heat flux divergence associated with the weakened warm LC eddy. The anomalous surface warming is largest in the northern GoM due to the reduced SST warming and thus the reduced latent cooling there (not shown).

5. Weakening of the AMOC and the Loop Current

Figure 4a shows the seasonal cycle of the volume transport across the Yucatan Channel for the three different periods obtained from EXP_HR. The volume transport is reduced drastically from 24 Sv to 19 Sv, which is about a 25% decrease, by the late 21st century. As shown in Figure 4b and c, the AMOC is also significantly reduced in the late 21st century, consistent with Schmittner et al. [2005]. Since the LC is an important pathway of the AMOC, it is likely that the reduced LC in EXP_HR is driven by the deceleration of the AMOC.

The simulated volume transport of 24 Sv in the late 20th century (EXP_HR) agrees very well with the observed estimate of 23.8 ±1 Sv [e.g., Sheinbaum et al., 2002]. This means that the downscaled model with the horizontal resolution of 0.1 degree is quite sufficient to capture the mean strength of the LC volume transport. In EXP_LR, on the other hand, the simulated LC volume transport is only about 9 Sv in the late 20th century, which is unrealistically smaller than the observed estimate, and decreases to 7 Sv by the late 21st century. These results from EXP_LR are consistent with the IPCC-AR4 model simulations. Note that the simulated LC volume transport in the eleven IPCC-AR4 model simulations for the 20th century is only about 4 – 12 Sv. Among the eleven IPCC-AR4 models, only five models (MRI_CGCM2, GISS_MODEL_E_R, MPI_ECHAM5, MIUB_ECHO_G, GISS_AOM) show the reduction of LC volume transport to some extent. It appears that the insufficient number of the model grid points across the Yucatan Channel prevents the IPCC-AR4 models and EXP_LR from properly simulating the mean strength of the LC volume transport and its reduction in the 21st century.

In the next section, we explore how this reduction of the LC in EXP_HR affects the basin-wide warming of the GoM in the 21st century.

6. Cooling effect of the reduced Loop Current

The LC is important for the upper ocean heat budget of the GoM because it carries the warm Caribbean water into the GoM and thus maintains the warmth of GoM. Consistently, the advective flux convergence for the whole column in the GoM during the late 20th century is positive in both EXP_HR (55 TW, 1TW = 10^{12}W) and EXP_LR (25 TW) as summarized in Table 2. Thus, the LC transport in both EXP_HR and EXP_LR has a warming influence to the GoM over the year whereas the net surface flux has a cooling influence over the year and offsets the warming effect by the LC. As shown in Figure 5d, the advective heat flux convergence plays an important role in the GoM in EXP_HR since the LC carries warmer water from Caribbean

Sea into the GoM especially in spring and early summer, thus offsetting the surface cooling in GoM during winter.

In EXP_LR, on the other hand, the advective heat flux convergence only plays a minor role in the GoM due to unrealistically weak LC. Figures 5b and 5e show the anomalous (i.e., late 21st century – late 20th century) seasonal cycle of heat budget terms averaged in the GoM for EXP_LR and EXP_HR, respectively. The combined effect of anomalous surface flux and advective heat flux convergence results in the warming of GoM. As summarized in Table 2, the surface flux increases more in EXP_HR (5.0 TW) than that in EXP_LR (3.1 TW), but the advective heat convergence increases much less in EXP_HR (3.9 TW) than that in EXP_LR (7.3 TW). Particularly from late summer to spring months (September – March), in EXP_HR, the GoM is subject to anomalous advective heat flux *divergence* (i.e., $\Delta Q_{ADV} < 0$) as shown in Figure 5e. However, in EXP_LR, the GoM is influenced by anomalous advective heat flux *convergence* (i.e., $\Delta Q_{ADV} > 0$) year-around (Figure 5b).

In order to understand how the reduced LC may affect the heat budget of the GoM, it is important to explore more about the anomalous advective heat convergence (ΔQ_{ADV}, LHS) into the GoM, which can be given by

$$\Delta Q_{ADV} = \underbrace{\rho c_p V \Delta \delta T}_{\Delta Q_{\delta T}} + \underbrace{\rho c_p \Delta V \delta T}_{\Delta Q_V} + \underbrace{\rho c_p \Delta \delta T \Delta V}_{\Delta Q_{\delta TV}}, \quad (2)$$

where ρ is the seawater density, c_p is the specific heat of seawater, V is the volume transport across the Yucatan Channel (or Florida Channel), δT is the temperature difference between the Yucatan Channel and Florida Straits (i.e., $T_{YUC} - T_{FLO}$), which is always positive, and ΔF represents the difference in the variable F between the late 21st century and the late 20th century.

The LHS is the anomalous advective heat flux convergence (ΔQ_{ADV}). The RHS shows all the contributing terms of ΔQ_{ADV} (i.e., $\Delta Q_{\delta T}$, ΔQ_V and $\Delta Q_{\delta TV}$). The second term on the RHS of (2), which is referred to as ΔQ_V, is negative if the LC is reduced (i.e., $\Delta V < 0$). Therefore, the reduced LC results in anomalous advective heat flux divergence in the GoM, and thus cools the GoM basin. However, the first term in the RHS, which is referred to as $\Delta Q_{\delta T}$, is positive in both EXP_HR and EXP_LR and dominates the other term as summarized in Table 3. Therefore, the GoM is affected by anomalous advective heat flux convergence (i.e., advective warming) during the 21st century. The positive value of $\Delta Q_{\delta T}$ is associated with the increased δT during the 21st century (see equation 2). Thus, the water that enters from the Caribbean Sea warms more than the water that exits through the Florida Straits. The third term is the nonlinear term ($\Delta Q_{\delta TV}$), which is smaller than other two terms.

The advective heat budget summarized in Table 3 (for annual mean and Table 4 for MAM season) clearly indicates that the anomalous advective heat flux convergence in the GoM is too high in EXP_LR (7.3 TW in EXP_LR versus 3.9 TW in EXP_HR) because the basin-wide cooling associated with the reduced LC (ΔQ_V) is too small in EXP_LR (-3.5 TW in EXP_LR versus -11.7 TW in EXP_HR).

Figure 5c and 5f show the anomalous (i.e., late 21st century – late 20th century) seasonal cycle of advective heat convergence and all the contributing terms ($\Delta Q_{\delta T}$, ΔQ_V and $\Delta Q_{\delta TV}$) averaged in the GoM for EXP_LR and EXP_HR, respectively. The cooling associated with the reduced LC (ΔQ_V) is large and thus plays an important role in EXP_HR, especially in spring and early summer, whereas ΔQ_V in EXP_LR is much smaller and thus not an important player, clearly explaining why the GoM is warmed more in EXP_LR than in EXP_HR. In other words, the cooling associated with the reduced LC (ΔQ_V) is underestimated in EXP_LR because the LC reduction during the 21st century is only 1.6 Sv in EXP_LR, whereas it is 4.7 Sv in EXP_HR.

7. Summary and Discussions

In this paper, we examine the potential impact of future AGW on the GoM by using a high-resolution MICOM-AML constrained with the surface forcing fields and initial and boundary conditions obtained from the IPCC-AR4 model simulations under A1B scenario. The LC transport has a net warming influence on the GoM, whereas the net surface flux has a net cooling influence and thus offsets the warming influence of the LC. The simulated volume transport across the Yucatan Channel (and the Florida Channel) is reduced by 20 - 25% during the 21st century, consistent with a similar rate of reduction in the AMOC. The reduced LC and the associated weakening of the warm LC eddy have a cooling impact in the GoM, particularly in the northern GoM. Therefore, the northern GoM where LC eddies predominate is characterized as the region of minimal warming. Low-resolution models, such as the IPCC-AR4 models, underestimate the reduction of the LC and its cooling effect, thus fail to simulate the reduced warming feature in the northern GoM.

The reduced warming in the northern GoM will have important implications for marine ecosystems, including the spawning of BFT in AMJ. Since the spawning of BFT is mainly temperature dependent and BFT are adversely affected by warm water, the reduced warming in the northern GoM will probably mitigate the IPCC-projected reduction in the areas of BFT spawning ground in the GoM [Muhling et al., 2011]. Therefore, it is essential to utilize downscaled models and reevaluate the potential effects of climate change on the spatial and temporal extent of BFT spawning in the GoM.

Finally, it is important to point out some of the limitations in this study. Here, we mainly focused on the temperature change in the GoM. Other factors including the salinity, the position and eddy-shedding process of LC should also be studied in detail in the future. Further research is also required on the ecosystem based-responses to climate changes in the GoM. This study will also benefit from the development of regional coupled atmosphere-ocean models.

Acknowledgements. We would like to thank Dr. Eric Des Barton and two anonymous reviewers for their thoughtful comments and suggestions, which led to a significant improvement of the paper. This work was supported by a grant from the National Oceanic and Atmospheric Administration Fishery and The Environment (FATE) program and a grant from the National Aeronautics and Space Administration.

References.

Blank, J. M., J. M. Morrissette, A. M. Landeira-Ferandez, S. B. Blackwell, T. D, Williams, and B. A. Block (2004), In situ cardiac performance of Pacific bluefin tuna hearts in response to acute temperaturechange. *J.Exp Biol*, 207, 881–890.

Bleck, R., C. Rooth, D. Hu, and L. T. Smith (1992), Salinity-driven thermocline transients in a wind- and thermohaline-forced isopycnic coordinate model of the North Atlantic. *J. Phys. Oceanogr.*, **22**, 1486–1505.

Carnes, M. R. (2009), Description and evaluation of GDEM-V 3.0, Tech. Rep. 724/NRL/MR/7300-09-9165, Nav. Res. Lab., Washington, D. C. (Available at http://www7320.nrlssc.navy.mil/pubs/pubs.php.)

Chassignet, E. P., L. T. Smith, R. Bleck, and F. O. Bryan (1996), A model comparison: Numerical simulations of the North and Equatorial Atlantic oceanic circulation in depth and isopycnic coordinates. *J. Phys. Oceanogr*., **26**, 1849-1867.

Drijfhout, S. S., and W. Hazeleger (2006), Changes in MOC and gyre-induced Atlantic Ocean heat transport. *Geophys. Res. Lett.,* **33,** L07707, doi:10.1029/2006GL025807.

Gaspar, P., (1988), Modeling the seasonal cycle of the upper ocean. *J. Phys. Oceanogr*., 18, 161-180.

Griffies, S. M., A. Biastoch, C. Boning, F. Bryan, E. Chassignet, G. Danabasoglu, M. H. England, R. Gerdes, H. Haak, R. W. Hallberg, W. Hazeleger, J. Jungclaus, W. G. Large, G. Madec, B. L. Samuels, M. Scheinert, C. A. Severijns, H. L. Simmons, A. M. Treguier, M. Winton, S. Yeager and J. Yin (2009), Coordinated Ocean-ice Reference Experiments (COREs). *Ocean Modell*., 26, 1-46.

Jaimes, B., L. K. Shay, and G. R. Halliwell (2011), The response of quasigeostrophic oceanic vortices to tropical cyclone forcing. *J. Phys. Oceanogr*., 41, 1965-1985.

Large, W.G. and S. G. Yeager (2008), The Global Climatology of an Interannually Varying Air-Sea Flux Data Set. *Clim. Dyn.,* doi:10.1007/s00382-008-0441-3.

Lee, S.-K., D. B. Enfield, and C. Wang (2005), Ocean General Circulation Model Sensitivity Experiments on the Annual Cycle of Western Hemisphere Warm Pool. *J. Geophys. Res*., 110, doi:10.1029/2004JC002640.

Lee, S.-K., D. B. Enfield., and C. Wang (2007), What Drives Seasonal Onset and Decay of the Western Hemisphere Warm Pool? *J. Climate*, 20, 2133-2146.

Lumpkin, R., and K. Speer (2007), Global Ocean Meridional Overturning. *J. Phys. Oceanogr.*, **37,** 2550–2562.

Muhling, B. A., S-K Lee., J. T. Lamkin., and Y. Liu (2011), Predicting the effects of climate change on bluefin tuna (Thunnus thynnus) spawning habitat in the Gulf of Mexico. – *ICES J. Mar. Sci.*, doi:10.1093/icesjms/fsr008.

Oey, L-Y., T. Ezer, and H. C. Lee (2005), Loop Current, rings and related circulation in the Gulf of Mexico: A review of numerical models and future challenges. *In Circulation in the Gulf of Mexico: Observations and Models*, Washington, DC, AGU, 31-56.

Price, R., A. Weller, and R. Pinkel (1986), Diurnal cycling: Observations and models of the upper ocean response to diurnal heating, cooling, and wind mixing. *J. Geophys. Res*., 91, 8411–8427.

Schaefer, K. M. (2001), Reproductive biology. In: *Tunas: Physiology, ecology and evolution* B.A. Block, E.D. Stevens (eds). San Diego, California: Academic Press. pp. 225-270.

Schmittner, A. (2005), Decline of the marine ecosystem caused by a reduction in the Atlantic overturning circulation. *Nature*, 434, 628-633.

Schmittner, A., M. Latif, and B. Schneider (2005), Model Projections of the North Atlantic thermohaline circulation for the 21st century assessed by observations. *Geophys. Res. Lett.*, 32, L23710, doi:10.1029/2005GL024368.

Seager, R., M. B. Blumenthal, and Y. Kushnir (1995), An Advective Atmospheric Mixed Layer Model for Ocean Modeling Purposes: Global Simulation of Surface Heat Fluxes. *J. Climate*, 8, 1951–1964.

Sheinbaum, J., J. Candela, A. Badan, and J. Ochoa (2002), Flow structure and transport in Yucatan Channel, *Geophys. Res. Lett*., 29 (3), 1040, doi:10.1029/2001GL013990.

Figure Captions

Figure 1. SST difference in the GoM between the late 21st century and late 20th century during AMJ obtained from (a) the weighted ensemble of 11 IPCC-AR4 models, (b) the low-resolution MICOM experiment (EXP_LR) and (c) the high-resolution MICOM experiment (EXP_HR). The unit for the temperature is K.

Figure 2. (a) Long-term mean surface current in the late 20th century during AMJ obtained from EXP_HR. (b) Anomalous (i.e., late 21st century – late 20th century) surface current in the GoM during AMJ obtain from EXP_HR.

Figure 3. (a) Anomalous (i.e., late 21st century – late 20th century) surface heat flux in the GoM during MAM obtained from EXP_HR. (b) Anomalous (i.e., late 21st century – late 20th century) advective heat flux convergence (colored) and surface current (vector) in the GoM during MAM obtained from EXP_HR. The unit for the heat flux terms is W/m^2.

Figure 4. (a) Seasonal cycle of the volume transport (Sv) across the Yucatan Channel for three different periods (the late 20th century, the mid 21st century and the late 21st century) obtained from EXP_HR. Time-averaged Atlantic MOC in (b) the late 20th century and (c) the late 21st century obtained from EXP_HR.

Figure 5. Seasonal cycle of heat budget terms averaged in the GoM (a) for EXP_LR in the late 20th century and (d) EXP_HR in the 20th century. Anomalous (i.e., late 21st century – late 20th century) seasonal cycle of heat budget terms averaged in the GoM (b) for EXP_LR and (e)

EXP_HR. Anomalous (i.e., late 21st century – late 20th century) seasonal cycle of advective heat convergence and all the contributing terms ($\Delta Q_{\delta T}$, ΔQ_{V} and $\Delta Q_{\delta TV}$) averaged in the GoM (c) for EXP_LR and (f) EXP_HR.

Table 1. The weight of each IPCC-AR4 model used to derive the surface flux fields and initial and boundary conditions for the MICOM-AML simulations.

Rank	**Model**	**Model Weight**
1	CSIRO_MK3_5	1.67
2	MRI_CGCM2_3_2A	1.50
3	GISS_MODEL_E_R	1.17
4	MPI_ECHAM5	1.07
5	NCAR_CCSM3	1.02
6	GFDL_CM2_1	1.00
7	MIROC3_2_MEDRES	0.94
8	MIUB_ECHO_G	0.88
9	GISS_AOM	0.86
10	GFDL_CM2_0	0.70
11	IPSL_CM4	0.17

Table 2. Annual heat budget terms (Q_{NET}: surface heat flux; Q_{ADV}: advective heat flux convergence; and Q_{STR}: heat storage rate) averaged in the GoM for the late 20th century, the late 21st century and the difference between the two periods obtained from EXP_HR and EXP_LR. The unit for the heat flux terms is TW.

Period Experiment	Late 20C (EXP_HR)	Late 21C (EXP_HR)	Difference (EXP_HR)	Late 20C (EXP_LR)	Late 21C (EXP_LR)	Difference (EXP_LR)
Q_{NET}	-54.6	-49.6	5.0	-24.4	-21.4	3.1
Q_{ADV}	54.9	58.8	3.9	24.9	32.2	7.3
Q_{STR}	0.3	9.2	8.9	0.5	10.9	10.4

Table 3. Anomalous advective heat flux convergence ΔQ_{ADV} in the GoM and all the contributing terms in the EXP_HR and EXP_LR experiments. $\Delta\delta T$ is the temperature difference between the Yucatan Channel and Florida Straits (i.e., $T_{YUC} - T_{FLO}$) in the late 21st century minus that during the late 20th century, and ΔV is volume transport change between the late 20th and the 21st century. The unit for the heat flux terms is TW.

Experiment	ΔQ_{ADV}	$\Delta Q_{\delta T}$	ΔQ_V	$\Delta Q_{\delta TV}$	$\Delta\delta T$ (°C)	ΔV (Sv)
EXP_HR	3.9	19.5	-11.7	-3.9	0.26	-4.70
EXP_LR	7.3	12.5	-3.5	-1.7	0.34	-1.60

Table 4. Anomalous advective heat flux convergence ΔQ_{ADV} in the GoM and all the contributing terms in the EXP_HR and EXP_LR experiments during MAM season. The unit for the heat flux terms is TW.

Experiment	ΔQ_{ADV} (TW)	$\Delta Q_{\delta T}$ (TW)	ΔQ_{V} (TW)	$\Delta Q_{\delta TV}$ (TW)
EXP_HR	15.8	43.8	-18.8	-9.3
EXP_LR	18.1	25.7	-4.6	-2.9

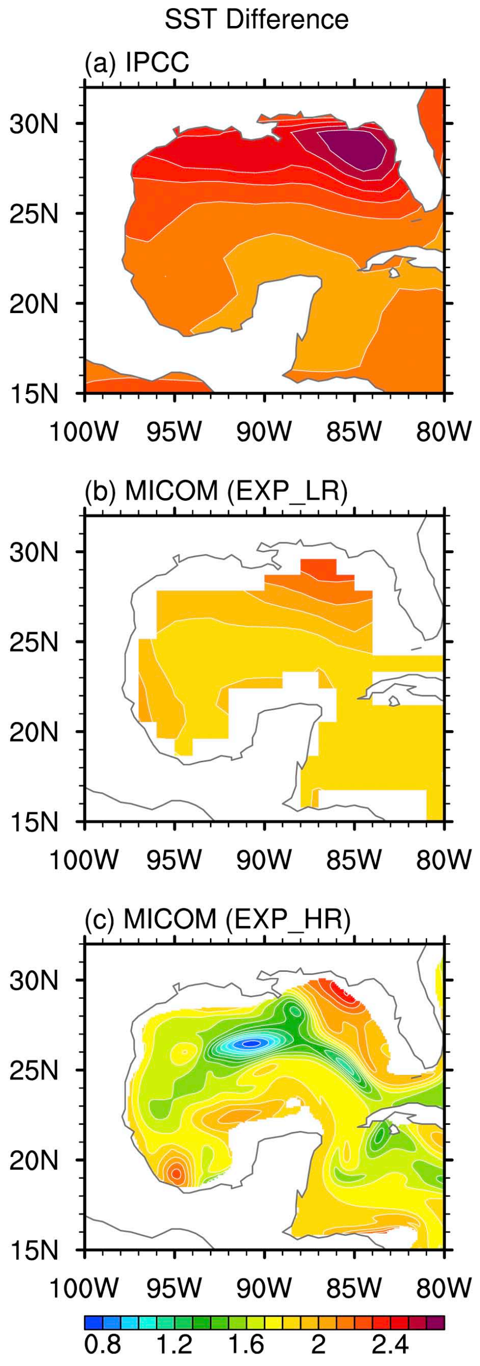

SST Difference
(a) IPCC
(b) MICOM (EXP_LR)
(c) MICOM (EXP_HR)
30N
25N
20N
15N
100W
95W
90W
85W
80W
0.8
1.2
1.6
2
2.4

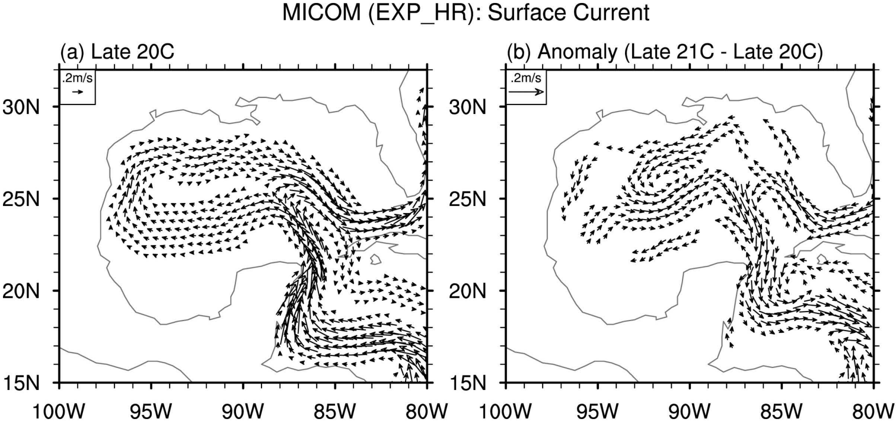
MICOM (EXP_HR): Surface Current
(a) Late 20C
(b) Anomaly (Late 21C - Late 20C)
.2m/s
.2m/s
30N
25N
20N
15N
100W
95W
90W
85W
80W

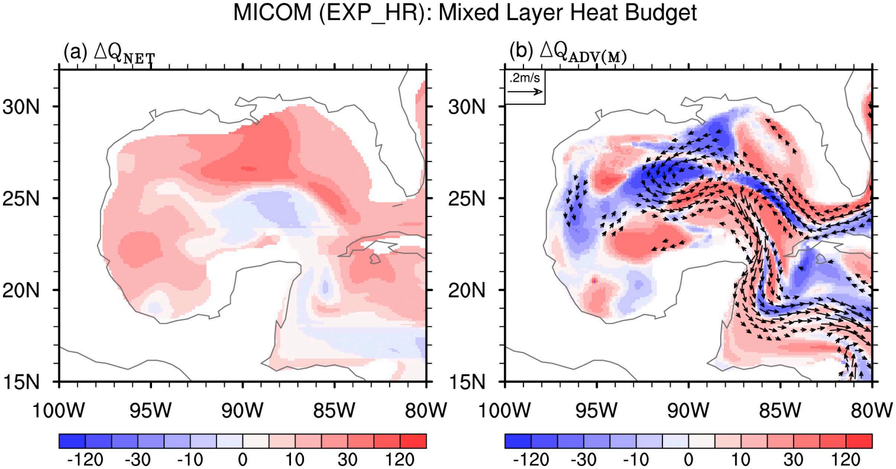

MICOM (EXP_HR): Mixed Layer Heat Budget
(a) ΔQ_{NET}
(b) $\Delta Q_{ADV(M)}$
.2m/s
30N
25N
20N
15N
100W
95W
90W
85W
80W
-120
-30
-10
0
10
30
120

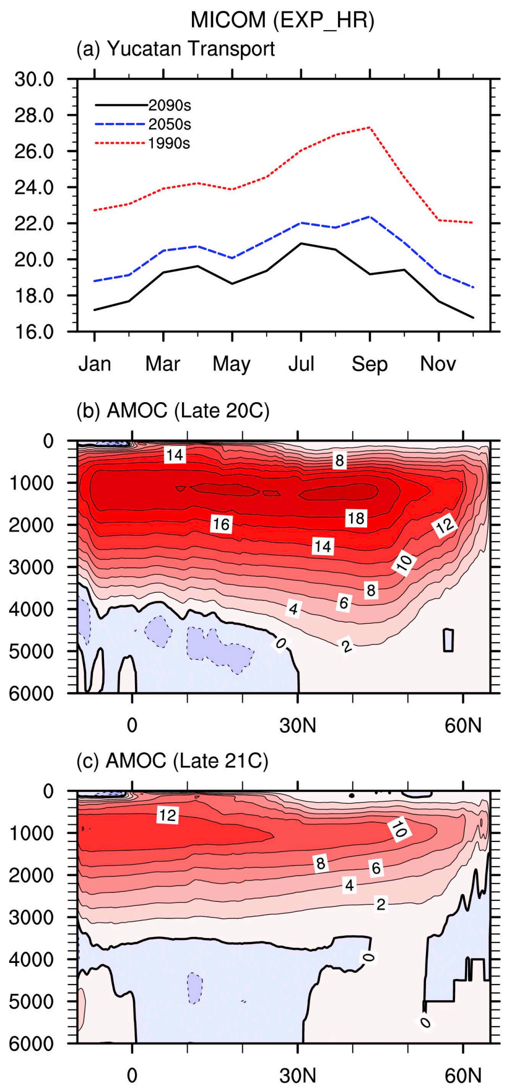
MICOM (EXP_HR)
(a) Yucatan Transport
2090s
2050s
1990s
30.0
28.0
26.0
24.0
22.0
20.0
18.0
16.0
Jan
Mar
May
Jul
Sep
Nov
(b) AMOC (Late 20C)
0
1000
2000
3000
4000
5000
6000
14
8
16
18
12
14
10
8
6
4
0
2
0
30N
60N
(c) AMOC (Late 21C)
12
10
8
6
4
2
0
0

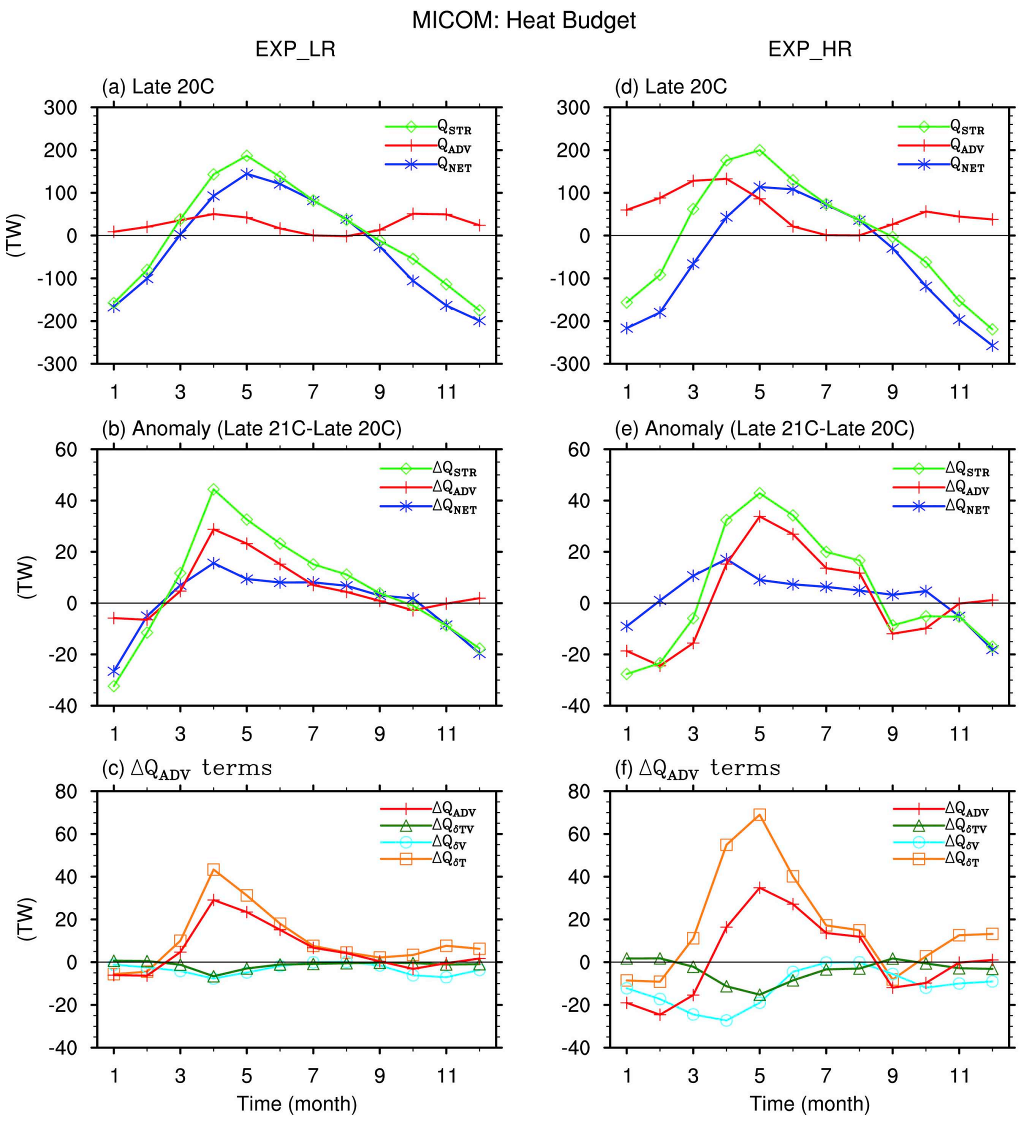
MICOM: Heat Budget
EXP_LR
EXP_HR
(a) Late 20C
(d) Late 20C
(b) Anomaly (Late 21C-Late 20C)
(e) Anomaly (Late 21C-Late 20C)
(c) ΔQ_ADV terms
(f) ΔQ_ADV terms
Q_STR
Q_ADV
Q_NET
ΔQ_STR
ΔQ_ADV
ΔQ_NET
ΔQ_δTV
ΔQ_δV
ΔQ_δT
(TW)
Time (month)